

REPORT DOCUMENTATION PAGE

Form Approved
OMB No. 0704-0188

Public reporting burden for this collection of information is estimated to average 1 hour per response, including the time for reviewing instructions, searching existing data sources, gathering and maintaining the data needed, and completing and reviewing the collection of information. Send comments regarding this burden estimate or any other aspect of this collection of information, including suggestions for reducing this burden, to Washington Headquarters Service, Directorate for Information Operations and Reports, 1215 Jefferson Davis Highway, Suite 1204, Arlington, VA 22202-4302, and to the Office of Management and Budget, Paperwork Reduction Project (0704-0188), Washington, DC 20503

AD-A219 975

1. AGENCY USE ONLY (Leave blank)	2. REPORT DATE Mar 90	3. REPORT TYPE AND DATES COVERED Journal Article
----------------------------------	--------------------------	---

4. TITLE AND SUBTITLE Theory of Magnetically Insulated Electron Flows in Coaxial Pulsed Power Transmission Lines	5. FUNDING NUMBERS 2301-F1-74
---	----------------------------------

6. AUTHOR(S) Robert I. Lawconnell Jesse Neri
--

7. PERFORMING ORGANIZATION NAME(S) AND ADDRESS(ES) F.J. Seiler Research Laboratory, US Air Force Academy CO 80840-6528 Naval Research Laboratory, Washington DC 20375	8. PERFORMING ORGANIZATION REPORT NUMBER FJSRL-JR-90-0005
--	--

9. SPONSORING / MONITORING AGENCY NAME(S) AND ADDRESS(ES)	10. SPONSORING / MONITORING AGENCY REPORT NUMBER
---	--

DTIC
ELECTE
APR 02 1990
S E E D

11. SUPPLEMENTARY NOTES

12a. DISTRIBUTION / AVAILABILITY STATEMENT Distribution Unlimited	12b. DISTRIBUTION CODE
--	------------------------

13. ABSTRACT (Maximum 200 words) The Cartesian magnetically insulated transmission line (MITL) theory of Mendel et al [Appl. Phys. 50, 3830 (1979); Phys. Fluids 26, 3628 (1983)] is extended to cylindrical coordinates. A set of equations that describe arbitrary electron flows in cylindrical coordinates is presented. These equations are used to derive a general theory for laminar magnetically insulated electron flows. The laminar theory allows one to specify the potentials, fields, and densities across a coaxial line undergoing explosive electron emission at the cathode. The theory is different from others available in cylindrical coordinates in that the canonical momentum and total energy for each electron may be nonzero across the electron sheath. A nonzero canonical momentum and total energy for the electrons in the sheath allows the model to produce one-dimensional flows that resemble flows from lines with impedance mismatches and perturbing structures. The laminar theory is used to derive two new self-consistent cylindrical flow solutions: (1) for a constant density profile and (2) for a quadratic density profile of the form $p = p_c [r_m^2 - r^2] / (r_m^2 - r_c^2)$. This profile is of interest in that it is similar to profiles observed in a long MITL simulation [Appl. Phys. 50, 4996 (1979)]. The theoretical flows are compared to numerical results obtained with 2-D electromagnetic particle-in-cell codes.

14. SUBJECT TERMS Pulse Power; Magnetic Insulation; Transmission Lines.	15. NUMBER OF PAGES 12
--	---------------------------

16. PRICE CODE

17. SECURITY CLASSIFICATION OF REPORT UNCLASSIFIED	18. SECURITY CLASSIFICATION OF THIS PAGE UNCLASSIFIED	19. SECURITY CLASSIFICATION OF ABSTRACT UNCLASSIFIED	20. LIMITATION OF ABSTRACT NONE
---	--	---	------------------------------------

$$f_{sub} = [(r_{sub} - r_{sub}) / (r_{sub} - r_{sub})]$$

Theory of magnetically insulated electron flows in coaxial pulsed power transmission lines

Robert I. Lawconnell

F. J. Seiler Research Laboratory, U. S. Air Force Academy, Colorado Springs, Colorado 80840

Jesse Neri

Naval Research Laboratory, Washington, DC 20375

(Received 6 October 1988; accepted 4 October 1989)

The Cartesian magnetically insulated transmission line (MITL) theory of Mendel *et al.* [Appl. Phys. 50, 3830 (1979); Phys. Fluids 26, 3628 (1983)] is extended to cylindrical coordinates. A set of equations that describe arbitrary electron flows in cylindrical coordinates is presented. These equations are used to derive a general theory for laminar magnetically insulated electron flows. The laminar theory allows one to specify the potentials, fields, and densities across a coaxial line undergoing explosive electron emission at the cathode. The theory is different from others available in cylindrical coordinates in that the canonical momentum and total energy for each electron may be nonzero across the electron sheath. A nonzero canonical momentum and total energy for the electrons in the sheath allows the model to produce one-dimensional flows that resemble flows from lines with impedance mismatches and perturbing structures. The laminar theory is used to derive two new self-consistent cylindrical flow solutions: (1) for a constant density profile and (2) for a quadratic density profile of the form $\rho = \rho_c [(r_m^2 - r^2)/(r_m^2 - r_c^2)]$. This profile is of interest in that it is similar to profiles observed in a long MITL simulation [Appl. Phys. 50, 4996 (1979)]. The theoretical flows are compared to numerical results obtained with two-dimensional (2-D) electromagnetic particle-in-cell (PIC) codes.



Accession For	
NTIS	GRA&I
DTIC TAB	<input checked="" type="checkbox"/>
Unannounced	<input type="checkbox"/>
Justification	
By _____	
Distribution/	
Availability Codes	
Dist	Avail and/or Special
A-1	20

I. INTRODUCTION

Magnetic insulation is essential in the operation of large pulsed power systems. This applies especially to systems with electric fields greater than approximately 20–50 MV/m because explosive electron emission occurs from surfaces subjected to such fields. These electrons will quickly short out the system in the absence of magnetic insulation. Therefore insuring magnetic insulation in large pulsed power systems is necessary for the transmission of the pulse to the load.

The principle of magnetic insulation is to externally apply or self-consistently generate magnetic fields that act perpendicular to the electric fields found in the system in order to confine the electrons. An example of magnetic insulation for a self-consistently generated magnetic field in a coaxial geometry is shown in Fig. 1. The current flowing in the system (I_a, I_e, I_c) generates a $-B_\theta$ field. The electric field is in the minus \hat{r} direction. As a result, the electrons emitted from the cathode plasma sheath are pulled by the imposed electric field toward the anode. However, the magnetic field redirects the electrons back toward the cathode by means of $\mathbf{v} \times \mathbf{B}$ forces. Therefore the electrons $\mathbf{E} \times \mathbf{B}$ drift in the $+\hat{z}$ direction while being magnetically insulated away from the anode. In Fig. 1, various electron orbit types are shown.² They are classified as common, laminar, curtate, and prolate. If the electrons are emitted from the cathode into a region in which the fields are uniform in z and the electrons initially have zero velocity, common orbits result. However, if the electrons are born in regions of nonuniform time varying fields, prolate, curtate, and laminar orbits can be pro-

duced. In many pulsed power systems, prolate, curtate, and laminar orbits dominate because of inherent field nonuniformities resulting from unavoidable perturbations in the magnetically insulated flows.

There are three different types of magnetically insulated (cutoff) flows³ referred to in the literature: (1) self-limited, (2) load-limited, and (3) constant-flux-limited flows. Load-limited magnetically insulated lines are of particular interest. An example of load-limited magnetic insulation is shown in Fig. 1. The current passing through the system is limited to that which passes through the load and is responsible for the insulation of the upstream region.

In the following, the theory of magnetically insulated

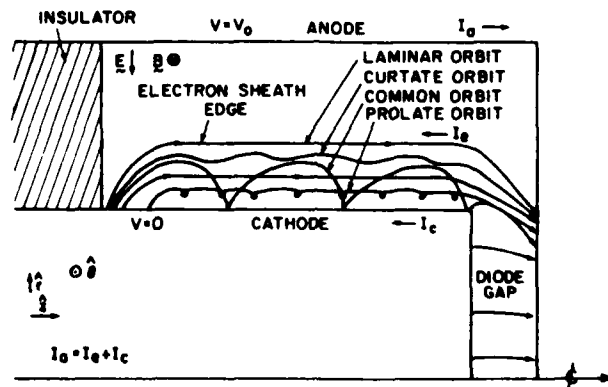


FIG. 1. Electron orbits in magnetically insulated flow. The primary electron orbits are shown along with the directions of the anode (I_a), cathode (I_c), and space charge (I_0) currents in a cylindrical geometry.

electron flows in cylindrical coordinates is extended to include flows with arbitrary distributions of canonical momentum and total energy (corresponding to self-limited and load-limited flows). In Sec. II, the basic physics governing the theoretical developments is presented. In addition, expressions for the drift velocity and sheath edge fields for electron flows with arbitrary electron orbits are obtained.

In Sec. III, laminar electron flows are considered and a general theory governing such flows in coaxial geometries is derived. It is found that for all laminar coaxial flows the relativistic factor for electrons at the sheath edge is given by $\gamma_m = I_a/I_c$. This is consistent with laminar and quasilaminar flows previously obtained.^{4,5}

In Sec. IV, the laminar theory is used to derive two new flow solutions: (1) a constant electron density flow and (2) a flow with a quadratic density profile of the form $\rho = \rho_c [(r_m^2 - r^2)/(r_m^2 - r_c^2)]$ [corresponding to a long magnetically insulated transmission line (MITL) simulation⁶]. In addition, it is shown how the Brillouin flow solution can be easily obtained from the general laminar theory. Finally, the flow solutions are compared.

In Sec. V, results from a particle-in-cell (PIC) code that emphasize the importance of laminar non-Brillouin flows are presented. Then the flow solutions are compared to PIC code simulations of coaxial load-limited magnetically insulated transmission lines (MITL). The constant density and quadratic density MITL solutions match the PIC code results more closely than the Brillouin flow solution. In Sec. VI, a summary of results is presented.

II. GENERAL THEORY

The theory of magnetic insulation begins with Hull's first Cartesian, nonrelativistic single-particle treatment of magnetron cutoff.⁷ In addition, much early nonrelativistic work was done in this area by Brillouin (Brillouin flow theory).⁸ Relativistic, self-consistent, Cartesian treatments began around 1973 when Lovelace and Ott found a condition governing constant-flux magnetic insulation of a diode.⁹ Also, at about this same time, Ron, Mondelli, and Rostoker (RMR) developed the "quasilaminar flow theory" employing common orbits (see Fig. 1) in Cartesian coordinates.¹⁰ In the work of RMR, it is assumed that the total energy and canonical momentum of each electron is equal to the total energy ($W = 0$) and momentum ($P_z = 0$) of an electron on the cathode. With this assumption, they find the electric and magnetic fields across the sheath, which are expressed nicely in terms of elliptic functions. A laminar flow theory for magnetically insulated transmission lines (MITL) was presented by Creedon in 1975 for Cartesian, cylindrical, and conical geometries.⁴ This theory also assumes that the total energy and canonical momentum of all electrons across the flow are equal to zero. It is commonly referred to as the Brillouin flow theory.^{4,8} Wang, in 1977, using a simple transformation, showed how the equations governing Brillouin flows could be transformed into Laplace's equation.¹¹ This allows for 2-D (arbitrary cathode/anode cross sections) Brillouin flows that are independent of the flow direction. In 1979, Mendel⁵ proposed a theory in Cartesian coordinates that allows the electrons to have arbitrary distributions of ca-

nonical momentum and total energy, taking into account a variety of electron orbits.

Many other papers have been written in the more mathematically tractable Cartesian coordinates¹²⁻¹⁷; unfortunately, a majority of experiments and applications involving magnetic insulation utilize cylindrical electrode geometries.¹⁸⁻²⁵ In practice, cylindrical systems can be rather accurately approximated by a Cartesian theory up to a vacuum impedance of about 15 Ω . For impedances larger than this cylindrical effects must be considered. For this reason, it is desirable to carry out new theoretical developments in cylindrical coordinates. Creedon and Wang were able to extend the laminar Brillouin flow theory to cylindrical coordinates. Bergeron did some nonrelativistic single species analysis of quasilaminar flows in which he showed that an equilibrium solution did not exist in the case of an inner cathode. In addition, he did two species work in coaxial geometries in which he developed a computational scheme capable of predicting self-consistent flows in the regions in which an equilibrium solution exists. His model is also capable of predicting the regions of existence or nonexistence of a solution.²⁶ Swegle attempted to extend the relativistic single species work of RMR to cylindrical coordinates, but once again found that an equilibrium "quasilaminar flow solution" did not exist.²⁷ In an APS talk,²⁸ Rosenthal and Mendel presented a pressure balance analysis in cylindrical coordinates and were able to obtain voltage contours for nonlaminar MITL flows with constant electron density profiles. This constitutes the first step in extending Mendel's Cartesian theory to cylindrical coordinates. This paper extends more of Mendel's work⁵ to cylindrical coordinates in a form that preserves information previously lost in the pressure balance approach. It also presents a general theory governing laminar magnetically insulated electrons flows in coaxial geometries. The laminar theory is different from others presented in cylindrical coordinates in allowing the canonical momentum and total energy of the electrons to be nonzero across the flow.

A. Basic physics

The electron flows in MITL's are often relativistic and collisionless. This is true for the electron flows being considered here. Therefore the relativistic Vlasov equation is used as a starting point for theoretical developments. It is given by Eq. (1):

$$\left(\frac{\partial}{\partial t} + \mathbf{v} \cdot \frac{\partial}{\partial \mathbf{x}} - e(\mathbf{E} + \mathbf{v} \times \mathbf{B}) \cdot \frac{\partial}{\partial \mathbf{p}} \right) f(\mathbf{x}, \mathbf{p}, t) = 0. \quad (1)$$

The relativistic electron momentum is

$$\mathbf{p} = \gamma m \mathbf{v} \quad (2)$$

and the relativistic weighting factor is

$$\gamma = (1 - \mathbf{v} \cdot \mathbf{v}/c^2)^{-1/2}. \quad (3)$$

Here \mathbf{v} is the directional velocity of the electron, $f(\mathbf{x}, \mathbf{p}, t)$ is the electron distribution function, \mathbf{E} is the electric field, and \mathbf{B} is the magnetic induction.

The \mathbf{E} and \mathbf{B} fields are self-consistently determined via Maxwell's equations:

$$\nabla \cdot \mathbf{B} = 0, \quad (4)$$

$$\nabla \times \mathbf{B} = -e\mu_0 \int d^3p \mathbf{v}f + \frac{1}{c^2} \frac{\partial}{\partial t} \mathbf{E}, \quad (5)$$

$$\nabla \cdot \mathbf{E} = -\frac{e}{\epsilon_0} \int d^3p f, \quad (6)$$

$$\nabla \times \mathbf{E} = -\frac{\partial \mathbf{B}}{\partial t}. \quad (7)$$

Assuming a steady-state solution allows one to drop the derivatives with respect to time in Eqs. (1), (5), and (7).

The physics embodied in the relativistic Lagrangian will be the basis for much of the following. The relativistic Lagrangian is

$$L = -mc^2/\gamma + e\varphi(\mathbf{x},t) - e\mathbf{v} \cdot \mathbf{A}(\mathbf{x},t), \quad (8)$$

where $\varphi(\mathbf{x},t)$ is the electrostatic potential and $\mathbf{A}(\mathbf{x},t)$ is the vector potential.

B. Gauss' and Ampère's laws in terms of the total energy and canonical momentum

The nature of the problem to be solved is shown in Fig. 1. A voltage difference (in the MV regime) is set across a coaxial transmission line and after a few nanoseconds a quasiequilibrium magnetically insulated state is established. The electrons that are emitted from the cathode in a space-charge-limited ($E_c = 0$) fashion enter a variety of orbits; common, curvate, prolate, laminar, etc., depending on nonuniformities in the fields.

Since the net flow of current inside the transmission line is in the $-\hat{z}$ direction (Fig. 1), and there is azimuthal symmetry, the magnetic field between the anode and cathode will be an r -dependent field in the $\hat{\theta}$ direction: $\mathbf{B} = B(r)\hat{\theta}$. In addition, the gradient of the applied potential yields an r -dependent electric field: $\mathbf{E} = E(r)\hat{r}$. Because an equilibrium state is being considered, all time-dependent terms are dropped at the start of the theoretical development.

Now, applying Gauss' law [from Eq. (6)] in conjunction with the relativistic Vlasov equation [Eq. (1)] implies (note that the following derivation partially extends the Cartesian treatment^{2,5} of Mendel *et al.* to cylindrical coordinates)

$$\begin{aligned} \nabla \cdot \mathbf{E} &= \nabla_r^2 \varphi(r) \\ &= -\frac{\rho(r)}{\epsilon_0} = \frac{e}{\epsilon_0} \int dp_z \int dp_r f(p_r, p_z), \end{aligned} \quad (9)$$

where $\nabla_r^2 = (1/r)\{(\partial/\partial r)[r(\partial/\partial r)]\}$, $\varphi(r)$ is the potential as a function of r across the transmission line, $\rho(r)$ is the electron charge density, ϵ_0 is the permittivity of free space, e is the electron charge, p_z and p_r are the z and r components of momentum, respectively, and $f(p_r, p_z)$ is the phase space electron density.

It is also true that if $\mathbf{B} = B(r)\hat{\theta}$ then

$$\nabla \times \mathbf{A} = \left(\frac{\partial}{\partial z} A_r - \frac{\partial}{\partial r} A_z \right) \hat{\theta}. \quad (10)$$

Since there is no electron flow loss in the radial direction there is no net radial electron flow as a function of r . This is because for every electron moving toward the cathode there is one moving toward the anode in every microscopic volume element. As a result $A_r = 0$. Therefore

$$B(r)\hat{\theta} = -\left(\frac{\partial}{\partial r} A_z \right) \hat{\theta}. \quad (11)$$

This means Ampère's law [Eq. (5)] becomes

$$\nabla \times \mathbf{B} = \nabla_z^2 A_z \hat{z} = \mu_0 \mathbf{J}. \quad (12)$$

To solve Eqs. (9) and (12) simultaneously requires a knowledge of the electron density and the current distribution defined in terms of the canonical momentum and total energy. First the canonical momentum and total energy will be defined using the cylindrical Lagrangian:

$$L = -mc^2[1 - (\dot{r}^2 + \dot{z}^2)/c^2]^{1/2} + e\varphi(r) - eA_z(r). \quad (13)$$

The z component of canonical momentum and momentum are, respectively,

$$p_{cz} = \frac{\partial L}{\partial \dot{z}} = m\dot{z} - eA_z(r) \quad (14)$$

and

$$p_z = m\dot{z} = p_{cz} + eA_z(r). \quad (15)$$

The r component of canonical momentum and momentum are given by

$$p_{cr} = \frac{\partial L}{\partial \dot{r}} = m\dot{r} = p_r. \quad (16)$$

The total energy is easily shown to be

$$w = (\gamma - 1)mc^2 - e\varphi(r). \quad (17)$$

Now, the electron density with canonical momentum between p_{cz} and $p_{cz} + dp_{cz}$ and energy between w and $w + dw$ at r is (from conservation of charge)

$$\frac{dn(p_{cz}, w)}{dp_{cz} dw} = \frac{1}{m^2 c^3} \frac{2|j(p_{cz}, w)|}{er}, \quad (18)$$

where $|j(p_{cz}, w)|$ is the one way current density per momentum interval per energy interval per radian (in azimuth) normalized to $m^2 c^3$. The factor of 2 comes from realizing that for every charge moving in the $+\hat{r}$ direction there is one moving in the $-\hat{r}$ direction. Here \dot{r} is a function of p_{cz} and w and is given by [see Eqs. (14) and (16)]

$$\dot{r}^2 = v^2 - z^2 = v^2 - (c/\gamma)^2 (p_{cz} + eA_z)^2. \quad (19)$$

Substituting in Eq. (3) and eliminating v^2 gives

$$\dot{r} = \frac{c}{\gamma} \left[\left(\frac{w + e\varphi mc^2}{mc^2} \right)^2 - 1 - \left(\frac{p_{cz} + eA_z}{mc} \right)^2 \right]^{1/2}. \quad (20)$$

Substituting (20) into (18) implies

$$d\rho(p_{cz}, w) = -e dn(p_{cz}, w) = -\frac{2|j(p_{cz}, w)|(w + e\varphi + mc^2)dp_{cz} dw}{(mc^2)^3 r \{ [(w + e\varphi + mc^2)/mc^2]^2 - 1 - [(p_{cz} + eA_z)/mc]^2 \}^{1/2}}. \quad (21)$$

The current density per momentum and energy interval is $d\rho$ times $\dot{z}(r)$. When one defines $\dot{z}(r)$ in terms of the total energy

and canonical momentum [from Eq. (14)] the current density is given by

$$dj(P_{cz}, W) = - \frac{2(p_{cz} + eA_z) |j(p_{cz}, w)| dp_{cz} dw}{m(mc^2)^2 r \{[(w + e\phi + mc^2)/mc^2]^2 - 1 - [(p_{cz} + eA_z)/mc]^2\}^{1/2}}. \quad (22)$$

Now, from Poisson's equation and Eq. (21)

$$\nabla_r^2 \phi = \frac{2}{\epsilon_0 (mc^2)^3} \int \int \frac{|j(p_{cz}, w)|(w + e\phi + mc^2) dp_{cz} dw}{r \{[(w + e\phi + mc^2)/mc^2]^2 - 1 - [(p_{cz} + eA_z)/mc]^2\}^{1/2}}. \quad (23)$$

From Ampère's law, the restrictions placed on the electron flow given earlier in this section, and Eq. (22), one obtains

$$\nabla_r^2 A_z = \frac{2}{\epsilon_0 (mc^2)^3} \int \int \frac{|j(p_{cz}, w)|(p_{cz} + eA_z) dp_{cz} dw}{r \{[(w + e\phi + mc^2)/mc^2]^2 - 1 - [(p_{cz} + eA_z)/mc]^2\}^{1/2}}. \quad (24)$$

The electron distribution function is defined to be

$$F(p_{cz}, w) \equiv \frac{2}{\epsilon_0 mc^2} |j(p_{cz}, w)|. \quad (25)$$

One should also note that in Eqs. (23) and (24), the integrals are performed in the canonical momentum and energy phase space. The variable r is independent of this space and can be pulled out of the integrals. In order to avoid rewriting the large integral arguments of (23) and (24) the following definition is given:

$$G(\phi, A_z) \equiv \int \int F(p_{cz}, w) \left[\left(\frac{w + e\phi + mc^2}{mc^2} \right)^2 - 1 - \left(\frac{p_{cz} + eA_z}{mc} \right)^2 \right]^{1/2} dp_{cz} dw. \quad (26)$$

This allows one to write (23) and (24) as

$$\nabla_r^2 \phi = \frac{1}{r} \frac{\partial G(\phi, A_z)}{\partial \phi} \quad (27)$$

and

$$c^2 \nabla_r^2 A_z = - \frac{1}{r} \frac{\partial G(\phi, A_z)}{\partial A_z}. \quad (28)$$

Now, multiplying Eq. (27) by $d\phi/dr$ and Eq. (28) by $-dA_z/dr$ and adding (with $d/dr \equiv '$) gives

$$[r(\phi'^2 - (cA_z')^2)]' + [\phi'^2 - (cA_z')^2] = 2G'.$$

Noting that $\phi' = -E(r)$ and that $A_z' = -B_\theta(r) = -B$ allows one to recast this equation as follows:

$$[r(E^2 - (cB)^2)]' + [E^2 - (cB)^2] = 2G'. \quad (29)$$

Another useful equation in the following work is obtained by multiplying Eq. (29) by r and regrouping:

$$[r^2(E^2 - (cB)^2)]' = 2[(rG)' - G]. \quad (30)$$

C. Expressions for drift velocity and sheath edge field

From the above, it is possible to obtain expressions for the electron drift and sheath edge electric field regardless of the electron orbit types. First, integrating Eq. (30) from the cathode (r_c) to the sheath edge (r_m) yields

$$r_m^2 [E_m^2 - (cB_m)^2] - r_c^2 [E_c^2 - (cB_c)^2] = -2 \int_{r_c}^{r_m} G dr = -P_m, \quad (31)$$

where the subscripts m and c refer to the sheath edge and cathode radii, respectively. Now, assuming space-charge-limited emission, $E_c = 0$. If one then writes Eq. (31) in terms of the anode and cathode currents with $B_m = \mu_0 I_a / 2\pi r_m$ and $B_c = \mu_0 I_c / 2\pi r_c$ (by Ampère's law, where I_c is the cathode current and I_a is the anode current),

$$E_m = - \frac{c\mu_0}{2\pi r_m} (I_a^2 - I_c^2)^{1/2} \times \left[1 - \left(\frac{2\pi}{c\mu_0} \right)^2 \frac{P_m}{(I_a^2 - I_c^2)} \right]^{1/2} \hat{r}, \quad (32)$$

where E_m is the electric field at the sheath edge (r_m). It is also true that if the electron charge per unit length is Γ , then

$$\Gamma = 2\pi\epsilon_0 r_m E_m, \quad \bar{v}_d \Gamma = I_a - I_c,$$

and therefore

$$E_m = [(I_a - I_c) / 2\pi\epsilon_0 r_m \bar{v}_d] \hat{r}, \quad (33)$$

where \bar{v}_d is the average drift velocity of the electron flow. From Eqs. (32) and (33) one sees that

$$\bar{v}_d = c \left(\frac{I_a - I_c}{I_a + I_c} \right)^{1/2} \left[1 - \left(\frac{2\pi}{c\mu_0} \right)^2 \frac{P_m}{(I_a^2 - I_c^2)} \right]^{-1/2}. \quad (34)$$

It is also obvious that the electric field at the anode is given by

$$E_a = r_m E_m / r_a. \quad (35)$$

III. LAMINAR THEORY

Up to this point, the theoretical developments have applied to all types of orbiting electrons. From this point on, laminar electron flows are considered. Laminar flows are characterized by electrons that have a zero r component of velocity. For laminar flows, the integrand of G [Eq. (26)] is zero; therefore P_m must be zero. Flows for which P_m is approximately zero may be common in numerical and real world experiments. A few MASK²⁹ calculations have been done in the 2 MV regime that indicate that often the electron drift velocities and fields only differ by a few percent from the laminar flow values. This is discussed in more detail in Sec. V, where the MASK calculations are presented. These simulations partially justify setting P_m equal to zero and de-

veloping a general laminar flow theory.

The laminar nature of the electron flows observed with MASK (discussed in Sec. V) in cylindrical coordinates is consistent with MAGIC³⁰ two-dimensional electromagnetic PIC code results done in Cartesian coordinates at Sandia. In the Sandia simulations, it was found that MITL flows in Cartesian coordinates are laminar in nature but non-Brillouin.³⁰ By non-Brillouin it is meant that the canonical momentum and total energy of the electrons are nonzero across the electron sheath. The assumption of a canonical momentum and total energy equal to zero across the sheath is fundamental to the well known Brillouin flow theory. In this paper, the non-Brillouin nature of the flow is ascertained in cylindrical coordinates by examining a laminar flow and comparing it to the Brillouin solution of Wang and Dicapua.³¹ In order to more accurately model laminar MITL flows in cylindrical coordinates a theory is developed in the next section that allows for nonzero canonical momentum and total energies across the flow.

A. Presentation of general laminar flow theory

The general theory is obtained via an interesting relation between the density and velocity profiles for relativistic MITL flows. A specification of the density profile implies a particular velocity profile and vice versa. This was first presented in a rather long derivation by one of the authors.³² A much simpler derivation is presented here utilizing Eq. (30) and Gauss' law. First, integrating (30) from the cathode to some arbitrary r with $G = 0$ implies

$$(rcB)^2 = (r_c c B_c)^2 + (rE)^2. \quad (36)$$

From Gauss' law one obtains

$$rE = \epsilon_0^{-1} \int_r^r \rho r dr = r_m E_m f(r), \quad (37)$$

which from (36) is

$$= [(r_m c B_m)^2 - (r_c c B_c)^2]^{1/2} f(r). \quad (38)$$

Finally, one notes for laminar flows ($dr/dt = 0$) that

$$v(r) = -E/B. \quad (39)$$

Therefore, if one substitutes Eqs. (36) and (38) into (39), the following equation results:

$$v(r) = c \{ (I_a^2 - I_c^2) f(r)^2 / [I_c^2 + (I_a^2 - I_c^2) f(r)^2] \}^{1/2} \hat{z}, \quad (40)$$

where I_a is the anode current, I_c is the cathode current, and $f(r)$ is the normalized weighted density profile and is given by

$$f(r) = \frac{\int_r^r \rho(r) r dr}{\int_r^m \rho(r) r dr}. \quad (41)$$

An interesting result easily proved using the above relations is that $\gamma_m = I_a/I_c$ at the sheath edge for all cylindrical laminar flow solutions. First one needs to note that $f(r_m) = 1$ at the sheath edge [see Eq. (41)]. In examining Eq. (41) one needs to realize that the integral $2\pi \int_r^m \rho(r) r dr$

is simply the total charge (q) in the sheath per unit length in z . From Eq. (32) with $P_m = 0$ and Gauss' law the total electron sheath space charge per unit length is given by

$$q = (I_a^2 - I_c^2)^{1/2} / c. \quad (42)$$

Substituting $f(r_m) = 1$ and q into Eq. (40) results in

$$V(r_m) = c(I_a^2 - I_c^2)^{1/2} / I_a,$$

which when substituted into the relativistic factor evaluated at the sheath edge results in

$$\gamma_m = I_a / I_c, \quad (43)$$

as expected.

B. Laminar flow equations

Given a density profile and the corresponding velocity profile [Eq. (40)], the self-consistent MITL flow solution is easily obtained via Maxwell's equations. The resulting equations are collected below in a convenient form. Given the charge density [$\rho(r)$] and the velocity [from Eq. (40)] the current density is

$$\mathbf{j} = \rho(r) \mathbf{v}(r). \quad (44)$$

The electric field is

$$\mathbf{E}(r) = \frac{\int_r^r \rho(r) r dr}{\epsilon_0 r} \hat{r} = r_m E_m \frac{f(r)}{r}, \quad (45)$$

where $\mathbf{E}(r_c) = 0$, because the cathode is a space charge limited emitter of electrons. The corresponding electrostatic potential is

$$\varphi(r) = - \int_r^r E(r) dr, \quad (46)$$

where $\varphi(r_c)$ is chosen to be zero. The magnetic induction is simply written as

$$\mathbf{B}(r) = \frac{\mu_0}{r} \left(\int_r^r j(r) r dr + \frac{I_c}{2\pi} \right) \hat{\theta}.$$

However, Eqs. (36) and (37) allow one to express $B(r)$ even more simply:

$$\mathbf{B}(r) = (\mu_0 I_c / 2\pi r) \{ 1 + [(I_a^2 - I_c^2) / I_c^2] f(r)^2 \}^{1/2} \hat{\theta}. \quad (47)$$

The vector potential is

$$\mathbf{A}(r) = - \int_r^r B(r) dr \hat{z}, \quad (48)$$

where $\mathbf{A}(r_c) = 0$ is chosen to equal zero at the cathode.

Now, from Eqs. (14), (17), (38), and (40) the canonical momentum and total energy of electrons at r are given by

$$\begin{aligned} p_{cz}(r) &= m\gamma v(r) - eA(r) \\ &= mc [rE(r) / r_c c B_c] - eA(r). \end{aligned} \quad (49)$$

The total energy is

$$\begin{aligned} w(r) &= -mc^2 \{ 1 - [1 - v^2(r)/c^2]^{-1/2} \} - e\varphi(r) \\ &= mc^2 [rB(r) / r_c B_c - 1] - e\varphi(r). \end{aligned} \quad (50)$$

If the sheath edge radius (r_m) in Eq. (41) is unknown it is easily found given I_a , I_c , the applied voltage across the gap

(V_a), and Eqs. (40), (45), and (46). From an experimental point of view, it is much more desirable to have the MITL flow as a function of I_a , I_c , and V_a rather than I_a , I_c , and r_m . This is because the applied voltage across the diode is usually known, but the outer sheath edge radius of the electron flow is not.

IV. LAMINAR THEORY APPLIED—TWO NEW SOLUTIONS

In order to demonstrate the general theory of laminar flows an outline of how one obtains the Brillouin flow solution from the above is included. Then two new MITL flow solutions are derived. The theory is used to generate a new self-consistent cylindrical MITL flow solution for flows with constant density profiles. This is done because in simulations of short MITL's, quasiconstant density profiles were observed. The theory is then used to produce a new analytic flow solution similar to that observed in a long MITL simulation.⁶ The density profile is given by a quadratic: $\rho = \rho_c [(r_m^2 - r^2)/(r_m^2 - r_c^2)]$. Finally, the constant density and Brillouin flow results are compared to a MASK simulation (Sec. V) of a short MITL. In addition, the quadratic MITL flow solution is compared with a long MITL simulation.

A. Outline of the Brillouin flow derivation

As a check on the theory of laminar flows derived in the previous section, one can use it to derive the well known Brillouin flow theory. Starting from Eqs. (26) and (29), while restricting the canonical momentum and total energy of each electron equal to zero, it is easy to show that the Brillouin density profile will have the following form:

$$\rho(r) = - (mc^2\epsilon_0/e)(A_n^2/r^2) \cosh[A_n \ln(r/r_c)]. \quad (51)$$

From Eq. (51), Eq. (41) becomes

$$f(r) = \sinh[A_n \ln(r/r_c)] / \sinh[A_n \ln(r_m/r_c)]. \quad (52)$$

With $f(r)$ given, the velocity is obtained from Eq. (40), the current density from Eq. (44), the electric field from (45), etc. If one carefully compares the resulting equations to those described by Wang and DiCapua³¹ it can be seen that the formulation and source of the constants is different but the Brillouin flow solution is reproduced.

B. Constant density flow

In various MASK calculations of short MITL's (Sec. V), it has been noted that the density as a function of radius is often relatively constant out to the sheath edge, where it drops to zero. For this reason, a self-consistent MITL flow solution for a constant density profile is given below in detail. Substituting a constant density profile into relation (41) and employing Eqs. (40) and (45)–(48) between $r_c < r < r_m$ result in

$$f(r) = (r^2 - r_c^2)/(r_m^2 - r_c^2), \quad (53)$$

$$\begin{aligned} v(r) = c \{ & (I_a^2 - I_c^2)(r^2 - r_c^2)^2 / [(I_a^2 - I_c^2) \\ & \times (r^2 - r_c^2)^2 + I_c^2(r_m^2 - r_c^2)^2] \}^{1/2}, \quad (54) \end{aligned}$$

$$\varphi(r) = (|\rho|/4\epsilon_0) [r^2 - r_c^2 - 2r_c^2 \ln(r/r_c)], \quad (55)$$

$$E(r) = [-|\rho|(r^2 - r_c^2)/2\epsilon_0 r] \hat{r}, \quad (56)$$

$$A(r) = -(\mu_0 I_c / 2\pi) K(r) \hat{z}, \quad (57)$$

and

$$B(r) = \frac{\mu_0 I_c}{2\pi r} \left[\left(\frac{I_a^2 - I_c^2}{I_c^2} \right) \left(\frac{r^2 - r_c^2}{r_m^2 - r_c^2} \right)^2 + 1 \right]^{1/2} \hat{\theta}, \quad (58)$$

where

$$K(r) = \frac{1}{2} \left[P(x) + \frac{b}{2a^{1/2}} \ln[2a^{1/2}P(x) + 2ax + b] - c_1^{1/2} \ln \left(\frac{2c_1^{1/2}P(x) + bx + 2c_1}{x} \right) \right]_{2z_c}^{2r}, \quad (59)$$

$$P(x) = (ax^2 + bx + c_1)^{1/2}, \quad a = c_3/4, \quad (60)$$

$$b = -c_3 r_c^2, \quad c_1 = c_3 r_c^4 + 1,$$

$$c_3 = [(I_a^2 - I_c^2)/I_c^2] (r_m^2 - r_c^2)^{-2}. \quad (61)$$

In a like manner the fields and flow quantities can easily be obtained from the sheath edge to the anode ($r_m < r < r_a$).

Next, one must consider the electron density profile. Thus far, all that is known is that it is constant out to the sheath edge where it drops to zero. The magnitude of the electron density and the sheath edge radius can be self-consistently determined from the theory. The electron density is obtained from Eqs. (32) and (56) evaluated at the sheath edge, which gives

$$\rho = - (I_a^2 - I_c^2)^{1/2} / c\pi(r_m^2 - r_c^2). \quad (62)$$

The sheath edge radius (r_m) is obtained by equating the expression for the potential at the anode to the anode voltage (V_a). The resulting expression is

$$\begin{aligned} \left(\frac{r_m}{r_c} \right)^{[1 - (r_c/r_m)^2]^{-1}} \\ = \frac{r_a}{r_c} \exp \left(0.5 - \frac{2\pi\epsilon_0 c V_a}{(I_a^2 - I_c^2)^{1/2}} \right). \quad (63) \end{aligned}$$

Therefore r_m is obtained iteratively given the anode and cathode currents, along with the anode and cathode radii, and the voltage difference across the diode. Once r_m is known all other quantities defined in Eqs. (53)–(62) are given. In typical experiments r_a , r_c , I_a , and V_a are known; I_c is a little harder to obtain, but can be found using a magnetic probe next to the cathode.³³

C. Quadratic flow

In 1979, Bergeron and Poukey⁶ presented PIC code results showing the electron density profile for long MITL's. The density profile is non-Brillouin in nature. In this section, the long MITL density profile is approximated by a quadratic:

$$\rho(r) = \rho_c [(r_m^2 - r^2)/(r_m^2 - r_c^2)]. \quad (64)$$

This relation is used in conjunction with Eqs. (40)–(50) to derive a self-consistent flow solution. In the region $r_c < r < r_m$, $f(r)$ is given by

$$f(r) = [r^2(2r_m^2 - r^2) - r_c^2(2r_m^2 - r_c^2)] / (r_m^2 - r_c^2)^2. \quad (65)$$

This quickly yields the velocity, current density, and electric and magnetic fields. To determine ρ_c we need only evaluate the relation for the electric field [integral form of Eq. (45)] at r_m and set it equal to the E_m given by Eq. (38). Following this procedure gives

$$\rho_c = -(2/c\pi) [(I_a^2 - I_c^2)^{1/2} / (r_m^2 - r_c^2)]. \quad (66)$$

To determine the sheath edge radius one integrates minus the electric field from the cathode to the anode and sets the potential thus obtained equal to the potential applied at the anode. The resulting equation can be solved iteratively for r_m and is given by

$$\left(\frac{r_m}{r_c}\right)^{[1 - (r_c^2/r_m^2)]^{-2}} \exp\left(\frac{1 - 3(r_m^2/r_c^2)}{4[(r_m^2/r_c^2) - 1]}\right) = \frac{r_a}{r_c} \exp\left(\frac{-2\pi\epsilon_0 V_a c}{(I_a^2 - I_c^2)^{1/2}}\right). \quad (67)$$

With r_m determined by (67) self-consistent solutions for flow with quadratic electron density profiles are obtained.

D. Comparison of the three flow solutions

In the following, the Brillouin flow, the constant, and the quadratic density MITL solutions are plotted together. The charge and current densities are shown in Figs. 2(a) and 2(b), respectively. The different MITL solutions have the following inputs:

$$I_a = 4.5 \times 10^5 \text{ A},$$

$$I_c = -2.43 \times 10^4 \text{ A},$$

$$V_a = 2.49 \times 10^6 \text{ V},$$

$$r_a = 0.08 \text{ m},$$

$$r_c = 0.07 \text{ m}.$$

The reason for comparing the flow solutions here is in order that one might see the differences in the flow solutions when all are applied self-consistently. In Sec. V, when the theory is compared to MASK simulations the Brillouin flow solutions cannot simultaneously match the currents and potentials observed in the simulations. This, of course, stems from the fact that the Brillouin flow solution is completely determined given the anode and cathode currents. The good thing about this is that the Brillouin solution can be used to predict the anode voltage given the anode and cathode currents (or given any two it can predict the third). The bad thing is that we may have trouble using it to match experimental and simulation results (to within a few percent, see Sec. V B) that have electrons whose canonical momentum and total energy change as a function of r , and therefore have non-Brillouin density and field profiles as well as differing values of the anode potential (given the currents).

In the following we note the similarities and differences in the three MITL solutions. In Fig. 2(a) the charge densities as a function of radius are compared. The Brillouin flow is the flow with the smallest sheath edge radius and most charge out close to the sheath edge. The quadratic MITL flow has the largest sheath edge radius and most charge next to the cathode. In Fig. 2(b), the greatest peak current density corresponds to the Brillouin flow and the lowest peak current density corresponds to the quadratic MITL flow. It is also interesting to note that the peak current density occurs at the sheath edge for the constant density and Brillouin flows, but about one-third of the way between the cathode and sheath edge for the quadratic MITL flow.

The electric and magnetic fields follow from the density profiles. As predicted by Eq. (32), with P_m equal to zero, the electric fields are the same from the outermost sheath edge to the anode. By Ampère's law the magnetic induction will be the same at the cathode and the same from the outermost sheath edge to the anode.

V. LAMINAR THEORY COMPARED TO SIMULATIONS

A computational tool based on Eqs. (1)–(7) is used to help justify the theoretical developments of Secs. II–IV. It is the two-dimensional electromagnetic particle-in-cell (PIC) code MASK.²⁹ First, it is used to generate electron orbit histories in typical load limited MITL's. These orbits are seen to be very laminar in nature (Fig. 3). In addition, Table I presents a few MASK calculations done in the 2 MV regime showing the percent difference of MASK's anode electric field from the laminar theory predictions. Then, Eq. (30) is used to evaluate, as a function of r across the MITL, the difference between MASK simulation (#5) and an arbitrary laminar flow (Fig. 4). The differences are once again small (except at the sheath edge), which partially justifies developing a general laminar flow theory. After checking simulation #5 to see that a laminar flow should model it well (data in Table

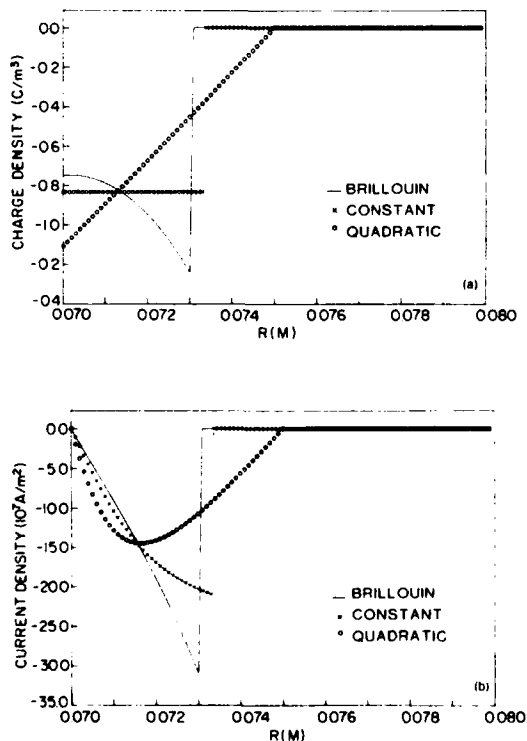


FIG. 2. Comparison of the charge and current density profiles for the Brillouin, constant density, and quadratic MITL flow solutions.

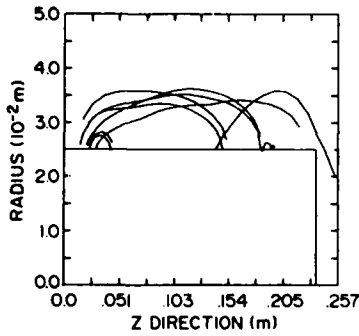


FIG. 3. The MASK semilaminar flow (simulation #0).

I and Fig. 4), its electric field and magnetic induction profiles are compared to the Brillouin and constant density flow profiles (Fig. 5). Finally, the quadratic MITL flow theory is compared to a simulation performed by Bergeron and Poukey (Fig. 6).⁶

A. Laminar nature of electron orbits

The laminar nature of electron orbits in a MITL is shown in Fig. 3. These electron orbits were generated using the PIC code MASK. The figure corresponds to an axial slice of a coaxial symmetric system with an interior cathode. The potential (V_a) across the cathode/anode gap is 2 MV, the diode gap (d_g) is 0.02 m, the cathode radius (r_c) and anode radius (r_a) are 0.025 and 0.05 m, respectively, and the anode current is 7.97×10^4 A.

It is clear that many of the emitted electrons are traveling 0.15–0.2 m before returning to the cathode. For common orbits (see Fig. 1), the electrons will travel approximately two Larmor radii in the \hat{z} direction before returning to the cathode. For this problem, the average Larmor radius is approximately $r_l = 0.0035$ m. This means the electrons are traveling approximately 60 Larmor radii in the \hat{z} direction before returning to the cathode. The electrons have little average radial momentum, and the flow is fairly well approximated by a laminar flow. Here Z -dependent electric field gradients along with a variety of other perturbations can result in such laminarlike flows.

The laminar nature of the electron orbits cited in the above example was typical of a large number of MASK simulations done in cylindrical coordinates. In Table I, the anode electric field for several calculations in the 2 MV regime are

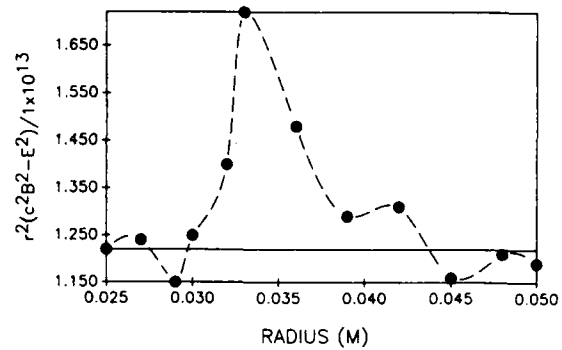


FIG. 4. Comparison of the quantity $r^2(c^2B^2 - E^2)$ from MASK (dashed-dotted curve) to what would be expected for a pure laminar flow [$(r_c c B_c)^2$ —the solid line] from the cathode to the anode.

compared to the laminar flow predictions. Even for MITL's with tightly trapped flows, load impedance one-third of self-limited impedance of the line, the anode electric fields only differ by 6% or 7% (see Table I) from the laminar flow solution. In examining the results of these MASK calculations it appears that the smaller the load impedance (the closer I_c comes to I_a), the larger the difference between the MASK and laminar flow predictions (see % Diff of Table I). This increase in % Diff has been noted to correspond to a larger percentage of electron orbits with smaller Larmor radii in the calculations. This is not surprising when one notes that the magnetic fields increase with decreasing loads (Z_l). The increase of structure in the flow should cause P_m (which is a measure of the laminar nature of the flow) of Eq. (31) to increase and as a result reduce the anode electric field from the expected laminar flow value. This is what one observes in Table I. Nevertheless since it is often desirable to run pulsed power devices with the largest possible load impedance while maintaining insulation, researchers often work close to the magnetic insulation limit of the MITL.^{31,32} In this region, the laminar theory's prediction of the anode electric field (E_a) differs from MASK by about a percent or less. Simulation #1 of Table I illustrates the situation in which the MITL is operated at the magnetic insulation threshold.^{31,32}

Finally, by integrating Eq. (30) from the cathode to some arbitrary r in the sheath, the difference between a laminar flow as a function of r and a PIC code simulation MASK simulation #5) is presented. These results are shown in Fig.

TABLE I. A comparison of the anode electric field obtained by MASK to that obtained using the laminar flow theory. These simulations are for a cathode radius of 0.025 m, anode radius of 0.05 m, and an applied potential of 2 MV. Here Z_l/Z_0 is the ratio of the load impedance over the line impedance. As this ratio decreases for the given voltage, it appears that the validity of the laminar flow assumption also decreases.

Simulation	I_a (A)	I_c (A)	Z_l/Z_0	E_a (V/m)	Laminar E_a	% Diff
1	7.96×10^4	-3.5×10^4	0.6	-8.5×10^7	-8.6×10^7	1.0
2	9.85×10^4	-8.4×10^4	0.5	-6.3×10^7	-6.2×10^7	-1.6
3	1.324×10^5	-1.215×10^5	0.36	-6.0×10^7	-6.3×10^7	5.0
4	1.56×10^5	-1.46×10^5	0.31	-6.1×10^7	-6.6×10^7	7.5
5	8.50×10^4	-5.81×10^4	0.57	-7.5×10^7	-7.4×10^7	0.8

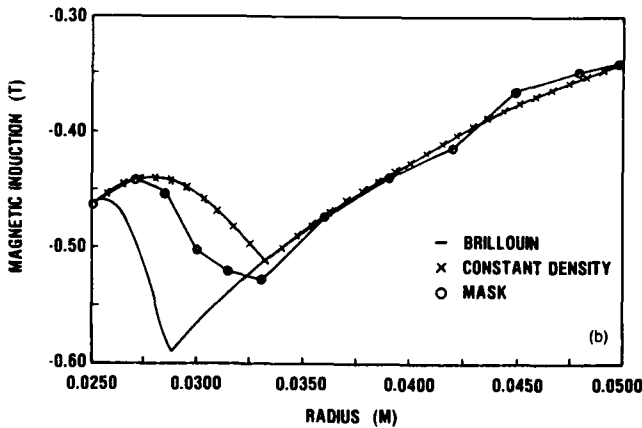
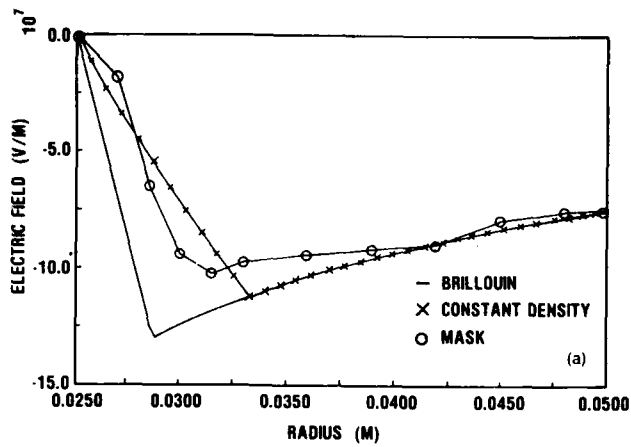


FIG. 5. A MASK short MITL simulation (#5) versus theory. (a) Electric field. (b) Magnetic induction.

4 and are representative of several MASK simulations. For laminar flows ($G = 0$) Eq. (36) implies

$$r^2(c^2B^2 - E^2) = (r_c c B_c)^2. \quad (68)$$

Now, the electric and magnetic fields along with r for simulation #5 are substituted into the left-hand side of Eq. (68) and are compared to the constant $(r_c c B_c)^2$. If the MASK simulation electron flow is completely laminar the difference between the left and right side of Eq. (68) would be zero. In Fig. 4, it can be seen that for simulation #5 excluding the sheath edge region the percent difference is not zero but is small: -5.5% – 7.0% different from the laminar flow prediction. The solid line of Fig. 4 corresponds to the pure laminar flow value. The dashed line corresponds to the MASK calculation. At the sheath edge, between 0.0315 and 0.036 m, the percent difference between the laminar flow prediction and the MASK simulation diverge (maximum difference of 40% for this simulation). This is being studied in greater detail, but may be due to appreciable values for G in the region, or it may simply be due to the inability of the code to resolve the fields in the sheath region for the given number of computational cells and particles. Nevertheless the simulation results indicate that the laminar flow assumption may

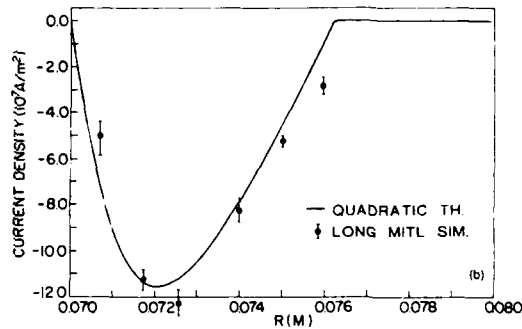
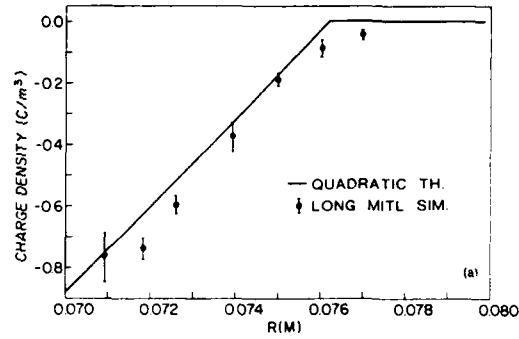


FIG. 6. Long MITL simulation³⁰ versus theory. (a) Charge density. (b) Current density.

often be appropriate and give results to within a few percent of the simulation (except perhaps at the sheath edge). As indicated in Table I, the laminar theory appears to be less applicable with tightly trapped flows (Z_1/Z_0 less than one-half the magnetic insulation threshold value).

B. Comparison of Brillouin and constant density solutions to a MASK simulation

In many short cylindrical MITL simulations, nonuniformities in the electric fields (usually E_z) sometimes result in laminar flows with density profiles that are nearly constant. In the following, MASK simulation #5 is compared to the constant density and Brillouin flow theories. The electric field and magnetic induction are compared as seen in Figs. 5(a) and 5(b), respectively. The simulation gave the following boundary conditions:

$$\begin{aligned} I_a &= 8.5 \times 10^4 \text{ A,} \\ I_c &= -5.813 \times 10^4 \text{ A,} \\ V_a &= 2.0 \times 10^6 \text{ V,} \\ r_a &= 0.05 \text{ m,} \\ r_c &= 0.025 \text{ m.} \end{aligned}$$

In Fig. 5(a), one should note that the electric field from the outermost sheath edge to the anode should match [see Eq. (32)] for a laminar flow. The Brillouin flow solution and the constant density solution do match. The MASK calculation is low out to about 0.038 m. From that point on, the MASK electric field oscillates about the laminar flow expected electric field. From the cathode to the sheath edge the

constant density flow solution more accurately predicts the electric field. The reason for this is that with the currents as specified, the Brillouin flow solution overestimates the applied potential. In fact, for this case the Brillouin flow corresponds to a potential of 2.31×10^6 V. This is off by about + 15.5% from that given in the simulation.

In Fig. 5(b), one notes that the constant density solution is doing a pretty good job of matching the magnetic fields of the simulation. One should note that the MASK magnetic induction oscillates about the constant density induction from the constant density sheath edge to the anode. It should also be noted that the constant density sheath edge is at 0.033 m, which corresponds rather closely to the MASK sheath edge. The Brillouin flow solution seems to be underestimating the distance from the cathode to the MASK sheath edge by nearly 50%.

C. Comparison of quadratic MITL solution to simulation

In 1979, Bergeron and Poukey did a series of simulations of long MITL's. In one of their papers⁶ they presented the charge and current density profiles of one simulation of interest. They also compared the simulation results to the Brillouin flow solution. It was a poor match except they noted that the areas under the curves were about the same. Now, the area under the charge density curve corresponds to the total charge per unit length, which was previously shown [in Eq. (42)] to be

$$q = (I_a^2 - I_c^2)^{1/2}/c.$$

The area under the current density curve corresponds to the total current (I_e) flowing within the sheath, which is simply

$$I_e = I_a - I_c.$$

Since I_a and I_c are the same for the simulation and the Brillouin flow solution the areas under the curves must be equal, assuming a laminar flow. This implies that the simulation done by Bergeron and Poukey may be modeled fairly accurately as a non-Brillouin laminar flow, which makes it of interest here.

In Figs. 6(a) and 6(b), the charge and current densities obtained in the simulation⁶ are compared to those predicted by the quadratic MITL solution [Eqs. (66)–(69), (40), and (44)]. The simulation gave the following boundary conditions:

$$I_a = 4.5 \times 10^5 \text{ A},$$

$$I_c = -2.4 \times 10^5 \text{ A},$$

$$V_a = 2.4 \times 10^6 \text{ V},$$

$$r_a = 0.08 \text{ m},$$

$$r_c = 0.07 \text{ m}.$$

It is clear from the figures that the theory is doing a fairly good job of matching the simulation results. It is doing a much better job than the Brillouin flow solution, which is shown for this case in Fig. 2.

Even though the quadratic MITL solution is much more consistent with the simulation than the Brillouin, the simulation results show a charge density distribution that is Gaussian in nature [Fig. 6(a)]. It is rounded at the cathode

and decreases slowly as the sheath edge is approached ending in a Gaussian tail. The profile used in this paper does not include the rounding at the cathode or the Gaussian tail at the sheath edge, although it does duplicate the gross features of the curve. As a result, the theory neglects the tail and underestimates the sheath edge radius. If one generated a function that fit the density profile of the simulation more closely, the laminar theory [Eqs. (40)–(50)] could be used to generate a better self-similar MITL flow solution for this long MITL.

VI. SUMMARY

Mendel's Cartesian MITL flow theory is partially extended to cylindrical coordinates. A set of equations that describe electron flows of arbitrary orbits in cylindrical coordinates is presented [Eqs. (29)–(35)]. The resulting equations are used to derive a new and general theory governing laminar flows in coaxial MITL's. This is done because many experiments are performed using coaxial systems in which laminar flows are believed to be important. It should be emphasized that in the new laminar theory the canonical momentum and total energy of the electrons are not restricted to zero across the electron sheath, as in the Brillouin theory. This allows one to consider one-dimensional electron flows that may have much in common with real world flows in which impedance mismatches and perturbing structures cause the electrons to have nonzero canonical momentum and total energy profiles.

The laminar flow theory is checked by considering the case in which each electron has zero canonical momentum and total energy across the flow—the well-known Brillouin flow theory results. The theory is then used to obtain a new analytic self-consistent MITL flow solution with a constant electron density profile. The constant density solution compares favorably with a short MITL MASK simulation (representative of several simulations). In addition, a new analytic flow solution with a quadratic density profile is presented. It is compared to a long MITL simulation and found to do a good job of matching flow quantities. The new flow solutions are compared with each other and with Brillouin flows. It is noted that the constant density and quadratic MITL solutions are more flexible than the Brillouin flow solution. It is also interesting to note that the theory predicts $\gamma_m = I_a/I_c$ at the sheath edge for all cylindrical laminar flows as expected.

This research can be applied to various additional areas. For instance, one could use the general theory to obtain the magnetic insulation threshold for a variety of non-Brillouin flows. The general theory could also be used to generate new laminar MITL flow solutions for a variety of electron density profiles. This might be especially useful to the researcher who intends to match simulation or experimental results to theory and is not satisfied with the Brillouin flow solution. The general theory could be used in conjunction with a PIC code to determine how laminar the flows from a given MITL are as a function of the radius. In this context, it could also be used to determine $G(r)$ for a given configuration. Finally, Eqs. (29)–(35) might be used to predict fields and flow vari-

ables in cylindrical pulsed power systems in which the fields and flow quantities are significantly affected by nonlaminar electron orbits.

ACKNOWLEDGMENTS

One of the researchers, R. Lawconnell, would like to thank P. Ottinger, J. Watrous, and J. Grossmann from the Naval Research Laboratory and J. McIver and N. Roderick from the University of New Mexico for many valuable discussions. In addition, the authors would like to thank the referee for all the useful comments and especially for suggesting the straightforward derivation of Eq. (40) in Sec. II [Eqs. (36)–(40)].

- ¹M. S. DiCapua, *IEEE Trans. Plasma Sci.* **11**, 205 (1983).
²C. W. Mendel, Jr., D. B. Seidel, and S. A. Slutz, *Phys. Fluids* **26**, 3628 (1983).
³J. M. Creedon, *Appl. Phys.* **48**, 1070 (1977).
⁴J. M. Creedon, *Appl. Phys.* **46**, 2946 (1975).
⁵C. W. Mendel, Jr., *Appl. Phys.* **50**, 3830 (1979).
⁶K. D. Bergeron and J. Poukey, *Appl. Phys.* **50**, 4996 (1979).
⁷A. W. Hull, *Phys. Rev.* **18**, 31 (1921).
⁸L. Brillouin, *Phys. Rev.* **67**, 260 (1945).
⁹R. V. Lovelace and E. Ott, *Phys. Fluids* **17**, 1263 (1974).
¹⁰A. Ron, A. A. Mondelli, and N. Rostoker, *IEEE Trans. Plasma Sci.* **PS-1**, 85 (1973).

- ¹¹M. Y. Wang, *Appl. Phys. Lett.* **33**, 284 (1978).
¹²M. P. Desjarlais and R. N. Sudan, *Phys. Fluids* **30**, 1536 (1987).
¹³P. A. Miller and C. W. Mendel, Jr., *Appl. Phys.* **61**, 529 (1987).
¹⁴R. C. Davidson, *Phys. Fluids* **28**, 377 (1985).
¹⁵C. W. Mendel, Jr., D. B. Seidel, and S. E. Rosenthal, *Laser Part. Beams* **1**, 311 (1983).
¹⁶M. P. Desjarlais and R. N. Sudan, *Phys. Fluids* **29**, 1746 (1986).
¹⁷K. D. Bergeron and J. W. Poukey, *Appl. Phys. Lett.* **27**, 58 (1975).
¹⁸J. P. Van Devender, *J. Appl. Phys.* **50**, 3923 (1979).
¹⁹J. P. Van Devender, J. P. Quintenz, R. J. Leeper, D. J. Johnson, and J. T. Crow, *Appl. Phys.* **52**, 4 (1981).
²⁰Kraft and M. W. McGeoch, *Phys. Fluids* **30**, 1189 (1987).
²¹E. I. Baranchikov, A. V. Gordeev, V. D. Korolev, and V. P. Smirnov, *Sov. Phys. JETP* **48**, 1058 (1978).
²²S. Shope, J. W. Poukey, K. D. Bergeron, D. H. McDaniel, A. J. Toepfer, and J. P. Van Devender, *Appl. Phys.* **49**, 3675 (1978).
²³S. Humphries, Jr., R. N. Sudan, and L. Wiley, *Appl. Phys.* **47**, 2382 (1976).
²⁴Y. Maron, *Phys. Fluids* **27**, 285 (1984).
²⁵I. D. Smith, P. Champney, and J. M. Creedon, in *Proceedings of the International Pulsed Power Conference*, Lubbock, Texas, *IEEE Catalog No. 76CH1147-8 Region 5* (IEEE, New York, 1976), Vol. II, p. c8-1.
²⁶K. D. Bergeron, *Phys. Fluids* **20**, 688 (1977).
²⁷J. A. Swegle, *Phys. Fluids* **25**, 1282 (1982).
²⁸S. E. Rosenthal and C. W. Mendel, *Bull. Am. Phys. Soc.* **30**, 1534 (1985).
²⁹A. T. Drobot, *Bull. Am. Phys. Soc.* **29**, 1379 (1984).
³⁰C. W. Mendel, Jr., J. A. Swegle, and D. B. Seidel, *Phys. Rev. A* **32**, 1091 (1985).
³¹M. Y. Wang and M. S. DiCapua, *Appl. Phys.* **51**, 5610 (1980).
³²R. I. Lawconnell, Ph.D. dissertation, University of New Mexico, 1988.
³³B. V. Weber (private communications, 1987).